Materials Letters 145 (2015) 145–149

Contents lists available at ScienceDirect

Materials Letters

journal homepage: www.elsevier.com/locate/matlet

A new phase in the Cu–Sn–Zn–S photovoltaic system

F. Boero [a], S. Delsante [a,*], D. Colombara [b], G. Borzone [a]

[a] Department of Chemistry and Industrial Chemistry, Genoa University, INSTM Consortium – UdR di Genova, via Dodecaneso 31, 16146 Genova, Italy
[b] Laboratory for Energy Materials - Université du Luxembourg, 41, rue du Brill, L-4422 Belvaux, Luxembourg

ARTICLE INFO

Article history:
Received 24 July 2014
Accepted 14 January 2015
Available online 22 January 2015

Keywords:
Cu–Sn–Zn–S system
Phase transformation
Microstructure
Scanning Electron Microscopy
Solar energy materials

ABSTRACT

More than 35 samples of the Cu–Zn–Sn–S system were prepared along the ZnS–Cu_2SnS_3 section, in order to study the bulk properties of the Cu_2ZnSnS_4 semiconductor. During the investigation of these samples, a new quaternary phase was detected by Scanning Electron Microscopy coupled with Energy Dispersive Spectroscopy (SEM/EDS) analyses. The results indicate that the new phase has a range of solubility corresponding to $Cu_{2-2x}Zn_{6+3x}Sn_{1-x}S_9$ with $0 < x < 0.74$ and decomposes at 790 °C as determined by Differential Thermal Analysis (DTA).

1. Introduction

Due to their semiconducting properties, chalcogenides have strong potential applications in industry, as demonstrated by the number of researchers who started studying them in the sixties. Recently, the importance of chalcogenides has increased, because they are used as absorber materials in thin film based solar cells. For this application only materials that display direct band-gap transitions can be employed, the best examples being $CuInSe_2$ (CIS), $CuIn_xGa_{1-x}Se_2$ with $0 \leq x \leq 1$ (CIGS) and CdTe. The record photovoltaic device efficiency for these materials is around 20% [1], but their use at terawatt (TW) scale is unlikely because of the scarce availability of some of the involved elements [2], of which Cd, Te and Ga also pose toxicity issues.

Therefore, among the possible Earth-abundant materials [3], the Cu–Zn–Sn–S system was proposed and, in particular, the Cu_2ZnSnS_4 phase (CZTS) is under investigation as a non-toxic, low cost alternative semiconductor. The main body of research on CZTS is focused on the deposition techniques and their impact on cell performance [4,5], as well as on the defect physics at thin film level [6], but there are a few studies on the bulk properties of this system. In order to fill this gap, more than 35 samples were prepared on the basis of the Cu–Zn–Sn–S phase diagram established by Olekseyuk et al. [7].

2. Experimental

Samples having different compositions that lie along the ZnS–Cu_2SnS_3 section were prepared starting from the powders of the pure elements (Cu 99.999, Zn 99.9, Sn 99.999, and S 99.9995 mass%) weighed with an accuracy of at least ±0.5 mg. The powders were pressed into pellets, sealed in quartz glass ampoules, and subjected to different thermal treatments to perform the synthesis. Two kinds of procedures have been employed: one based on the solid state synthesis reported by Choubrac et al. [8] and another based on high temperature heat treatments through the liquid phase (around 1000 °C) followed by annealing. All employed temperatures were selected on the basis of the phase diagram [7], see Table 1. Microstructures of the alloys were systematically investigated by light optical microscopy (LOM) on smooth samples prepared by grinding, lapping and polishing the resin-mounted samples with diamond abrasive spray down to 1 μm grain size. A thorough investigation of each sample with a Scanning Electron Microscope (SEM, Zeiss – EVO 40) was performed by using a backscattered electron detector (BSE) in order to reveal the compositional contrast between the different phases. Quantitative Electron Probe Micro-Analysis (EPMA) data were collected at 20 kV on a *Link system Ltd.* instrument equipped with an Energy Dispersive Spectroscopy (EDS) detector. A counting time of 100 s and the "ZAF" correction, a procedure in which corrections for atomic number effects (Z), absorption (A) and fluorescence (F) are calculated separately from suitable physical models programme, were adopted. Certified pure elements were used as reference standards, while cobalt was adopted for calibration purposes. The software package Inca Energy (Oxford Instruments, Analytical Ltd., Bucks, U.K.) was employed to process X-ray spectra. The EDS

* Corresponding author. Tel.: +39 010 3536160, +39 010 3536153; fax: +39 010 3625051.
E-mail address: simona.delsante@unige.it (S. Delsante).

http://dx.doi.org/10.1016/j.matlet.2015.01.048
0167-577X/

Table 1
Cu–Zn–Sn–S samples: nominal composition, synthetic route, SEM/EDS analysis and essential comments.

# Sample	Nominal composition	Heat treatment	Quaternary detected phases	SEM/EDS analysis				Comments
				Cu at%	Zn at%	Sn at%	S at%	
1	Cu_2ZnSnS_4	1000–960 °C and quenching	$Cu_{2-2x}Zn_{6+3x}Sn_{1-x}S_9$ Cu_2ZnSnS_4	11.4 24.8	33.4 13.3	5.6 12.3	49.6 49.6	70% Cu_2ZnSnS_4, 10% $Cu_{2-2x}Zn_{6+3x}Sn_{1-x}S_9$ Presence of eutectic (SnS–Cu_2S), SnS and Cu_2SnS_3.
2	Cu_2ZnSnS_4	500–600 °C and quenching	Cu_2ZnSnS_4	25.1	11.9	13.0	50.0	Around 70% Cu_2ZnSnS_4. Presence of eutectic (SnS–Cu_2S), Cu_2S, SnS, ZnS and Cu_2SnS_3.
3	Cu_2ZnSnS_4	500–1000 °C and quenching	$Cu_{2-2x}Zn_{6+3x}Sn_{1-x}S_9$ Cu_2ZnSnS_4	11.3 24.7	32.7 13.5	5.7 12.1	50.3 49.7	50% Eutectic (SnS–Cu_2S), 25% Cu_2ZnSnS_4, 20% $Cu_{2-2x}Zn_{6+3x}Sn_{1-x}S_9$. Presence of SnS and Cu_2SnS_3.
4	Cu_2ZnSnS_4	Quenching from 1050 °C	$Cu_{2-2x}Zn_{6+3x}Sn_{1-x}S_9$ Cu_2ZnSnS_4	3.0 26.7	44.5 10.6	1.4 12.8	51.1 49.9	50% Eutectic (SnS–Cu_2S), 25% $Cu_{2-2x}Zn_{6+3x}Sn_{1-x}S_9$, 20% Cu_2ZnSnS_4. Presence of SnS and Cu_2SnS_3.
5	Cu_2ZnSnS_4	1050–960 °C and quenching	$Cu_{2-2x}Zn_{6+3x}Sn_{1-x}S_9$ Cu_2ZnSnS_4	9.2 25.8	36.7 12.0	4.3 12.5	49.8 49.7	50% Eutectic (SnS–Cu_2S), 25% $Cu_{2-2x}Zn_{6+3x}Sn_{1-x}S_9$, 20% Cu_2ZnSnS_4. Presence of SnS and Cu_2SnS_3. See Fig. 1b.
6	Cu_2ZnSnS_4	1010–960 °C and quenching	$Cu_{2-2x}Zn_{6+3x}Sn_{1-x}S_9$ Cu_2ZnSnS_4	12.0 26.4	33.5 12.0	5.7 12.5	48.8 49.1	40% Eutectic (SnS–Cu_2S), 30% $Cu_{2-2x}Zn_{6+3x}Sn_{1-x}S_9$, 25% Cu_2ZnSnS_4. Presence of SnS and Cu_2SnS_3.
7	Cu_2ZnSnS_4	25–750 °C and quenching	Cu_2ZnSnS_4	25.1	13.3	12.5	49.1	More than 95% Cu_2ZnSnS_4. Presence of eutectic (SnS–Cu_2S).
8	Cu_2ZnSnS_4	25–750 °C, 750–400 °C and quenching	Cu_2ZnSnS_4	25.2	13.3	12.5	49.0	More than 95% Cu_2ZnSnS_4. Presence of SnS. See Fig. 1a.
9	Cu_2ZnSnS_4	25–750 °C and quenching	Cu_2ZnSnS_4	25.8	13.6	12.4	48.2	More than 95% Cu_2ZnSnS_4. Presence of eutectic (SnS–Cu_2S) and Cu_2S.
10	Cu_2ZnSnS_4	25–800 °C and quenching	Cu_2ZnSnS_4	25.2	13.5	12.4	48.9	More than 95% Cu_2ZnSnS_4. Presence of eutectic (SnS–Cu_2S) and Cu_2S.
11	Cu_2ZnSnS_4	Quenching from 1050 °C	$Cu_{2-2x}Zn_{6+3x}Sn_{1-x}S_9$ Cu_2ZnSnS_4	3.8 27.5	45.3 11.4	1.6 12.3	49.3 48.8	40% $Cu_{2-2x}Zn_{6+3x}Sn_{1-x}S_9$, 35% Cu_2ZnSnS_4. Presence of eutectic (SnS–Cu_2S), SnS and Cu_2SnS_3.
12	Cu_2ZnSnS_4	1050–1010 °C and quenching	$Cu_{2-2x}Zn_{6+3x}Sn_{1-x}S_9$ Cu_2ZnSnS_4	3.3 27.2	46.6 11.1	1.3 12.8	48.8 48.9	70% Cu_2ZnSnS_4, 20% $Cu_{2-2x}Zn_{6+3x}Sn_{1-x}S_9$. Presence of eutectic (SnS–Cu_2S), SnS and Cu_2SnS_3.
13	Cu_2ZnSnS_4	1050–960 °C and quenching	$Cu_{2-2x}Zn_{6+3x}Sn_{1-x}S_9$ Cu_2ZnSnS_4	7.9 26.5	39.8 12.2	3.5 12.5	48.8 48.8	45% Eutectic (SnS–Cu_2S), 30% Cu_2ZnSnS_4, 20% $Cu_{2-2x}Zn_{6+3x}Sn_{1-x}S_9$. Presence of SnS and Cu_2SnS_3.
14	$Cu_2Zn_2SnS_5$	1010–960 °C and quenching	$Cu_{2-2x}Zn_{6+3x}Sn_{1-x}S_9$ Cu_2ZnSnS_4	9.4 26.1	37.2 12.5	4.4 12.3	49.0 49.1	35% $Cu_{2-2x}Zn_{6+3x}Sn_{1-x}S_9$, 30% Cu_2ZnSnS_4. Presence of eutectic (SnS–Cu_2S), SnS and Cu_2SnS_3.
15	$Cu_4Zn_3Sn_2S_9$	1010–960 °C and quenching	$Cu_{2-2x}Zn_{6+3x}Sn_{1-x}S_9$ Cu_2ZnSnS_4	10.6 24.2	35.2 14.6	5.2 12.1	49.0 49.1	50% Cu_2ZnSnS_4, 45% $Cu_{2-2x}Zn_{6+3x}Sn_{1-x}S_9$. Presence of eutectic (SnS–Cu_2S) and SnS.
16	$Cu_4Zn_3Sn_2S_9$	1010–960 °C and quenching	$Cu_{2-2x}Zn_{6+3x}Sn_{1-x}S_9$ Cu_2ZnSnS_4	11.7 27.5	34.0 10.6	5.6 12.9	48.7 49.0	50% $Cu_{2-2x}Zn_{6+3x}Sn_{1-x}S_9$, 45% Cu_2ZnSnS_4. Presence of eutectic (SnS–Cu_2S), SnS and Cu_2SnS_3.
17	$Cu_2Zn_3SnS_6$	1010–960 °C and quenching	$Cu_{2-2x}Zn_{6+3x}Sn_{1-x}S_9$ Cu_2ZnSnS_4	7.9 26.7	39.2 11.9	3.8 12.6	49.1 48.8	80% $Cu_{2-2x}Zn_{6+3x}Sn_{1-x}S_9$, 10% Cu_2ZnSnS_4. Presence of eutectic (SnS–Cu_2S), SnS and Cu_2SnS_3.
18	$Cu_2Zn_3SnS_6$	1010–960 °C and quenching	$Cu_{2-2x}Zn_{6+3x}Sn_{1-x}S_9$ Cu_2ZnSnS_4	10.0 24.7	36.0 14.3	4.9 12.2	49.1 48.8	80% $Cu_{2-2x}Zn_{6+3x}Sn_{1-x}S_9$, 15% Cu_2ZnSnS_4. Presence of eutectic (SnS–Cu_2S) and SnS.
19	$Cu_2Zn_6SnS_9$	1010–960 °C and quenching	$Cu_{2-2x}Zn_{6+3x}Sn_{1-x}S_9$ Cu_2ZnSnS_4	3.1 25.9	44.6 11.5	1.5 12.7	50.8 49.9	60% $Cu_{2-2x}Zn_{6+3x}Sn_{1-x}S_9$, 20% Cu_2ZnSnS_4, 15% eutectic (SnS–Cu_2S). Presence of SnS.
20	$Cu_2Zn_6SnS_9$	Quenching from 1050 °C	$Cu_{2-2x}Zn_{6+3x}Sn_{1-x}S_9$ Cu_2ZnSnS_4	3.7 25.8	44.6 12.2	1.6 12.6	50.1 49.4	75% $Cu_{2-2x}Zn_{6+3x}Sn_{1-x}S_9$, 10% Cu_2ZnSnS_4, 10% eutectic (SnS–Cu_2S). Presence of SnS and Cu_2SnS_3.
21	$Cu_2Zn_6SnS_9$	1010–960 °C and quenching	$Cu_{2-2x}Zn_{6+3x}Sn_{1-x}S_9$ Cu_2ZnSnS_4	6.1 26.4	42.5 12.2	2.7 12.5	48.7 48.9	60% $Cu_{2-2x}Zn_{6+3x}Sn_{1-x}S_9$, 25% eutectic (SnS–$Cu_2S$), 10% Cu_2ZnSnS_4. Presence of SnS.
22	$Cu_2Zn_6SnS_9$	1010–960 °C and quenching	$Cu_{2-2x}Zn_{6+3x}Sn_{1-x}S_9$ Cu_2ZnSnS_4	7.2 27.2	40.4 11.6	3.5 12.5	48.9 48.7	85% $Cu_{2-2x}Zn_{6+3x}Sn_{1-x}S_9$, 10% Cu_2ZnSnS_4. Presence of eutectic (SnS–Cu_2S), SnS and Cu_2SnS_3.
23	$Cu_2Zn_6SnS_9$	1010–400 °C and quenching	$Cu_{2-2x}Zn_{6+3x}Sn_{1-x}S_9$ Cu_2ZnSnS_4	8.8 25.4	37.9 13.1	4.2 12.6	49.1 48.9	70% $Cu_{2-2x}Zn_{6+3x}Sn_{1-x}S_9$, 15% eutectic (SnS–$Cu_2S$), 10% Cu_2ZnSnS_4. Presence of Cu_2S and SnS.
24	$Cu_2Zn_6SnS_9$	25–940 °C and quenching.	$Cu_{2-2x}Zn_{6+3x}Sn_{1-x}S_9$ Cu_2ZnSnS_4	7.7 25.5	39.5 12.4	3.7 12.9	49.1 49.2	More than 95% $Cu_{2-2x}Zn_{6+3x}Sn_{1-x}S_9$. Presence of eutectic (SnS–Cu_2S) and Cu_2ZnSnS_4. See Fig. 2a.
25	$Cu_2Zn_6SnS_9$	25–960 °C and quenching.	$Cu_{2-2x}Zn_{6+3x}Sn_{1-x}S_9$ Cu_2ZnSnS_4	3.6 26.2	45.7 13.1	1.6 12.5	49.1 48.2	More than 95% $Cu_{2-2x}Zn_{6+3x}Sn_{1-x}S_9$. Presence of eutectic (SnS–Cu_2S), SnS and Cu_2ZnSnS_4.
26	$Cu_2Zn_6SnS_9$	Quenching from 1050 °C	$Cu_{2-2x}Zn_{6+3x}Sn_{1-x}S_9$ Cu_2ZnSnS_4	2.6 24.6	47.4 14.5	1.2 12.1	48.8 48.8	60% $Cu_{2-2x}Zn_{6+3x}Sn_{1-x}S_9$, 25% eutectic (SnS–$Cu_2S$), 10% Cu_2ZnSnS_4. Presence of SnS.
27	$Cu_2Zn_6SnS_9$	1050–1010 °C and quenching	$Cu_{2-2x}Zn_{6+3x}Sn_{1-x}S_9$ Cu_2ZnSnS_4	2.3 24.5	48.0 14.5	1.0 12.3	48.7 48.7	70% $Cu_{2-2x}Zn_{6+3x}Sn_{1-x}S_9$, 15% eutectic (SnS–$Cu_2S$), 10% Cu_2ZnSnS_4. Presence of SnS.
28	$Cu_2Zn_6SnS_9$	1050–960 °C and quenching	$Cu_{2-2x}Zn_{6+3x}Sn_{1-x}S_9$ Cu_2ZnSnS_4	3.4 26.3	46.4 12.5	1.4 12.4	48.8 48.8	80% $Cu_{2-2x}Zn_{6+3x}Sn_{1-x}S_9$, 10% eutectic (SnS–$Cu_2S$), 5% Cu_2ZnSnS_4. Presence of SnS.
29	$Cu_2Zn_6SnS_9$	1010–960 °C and quenching	$Cu_{2-2x}Zn_{6+3x}Sn_{1-x}S_9$ Cu_2ZnSnS_4	8.1 25.7	38.9 12.7	3.8 12.5	49.2 49.1	70% $Cu_{2-2x}Zn_{6+3x}Sn_{1-x}S_9$, 20% Cu_2ZnSnS_4. Presence of eutectic (SnS–Cu_2S), SnS and Cu_2SnS_3.
30	$Cu_2Zn_6SnS_9$	1010–960 °C and quenching	$Cu_{2-2x}Zn_{6+3x}Sn_{1-x}S_9$	8.1	38.8	3.9	49.2	More than 95% $Cu_{2-2x}Zn_{6+3x}Sn_{1-x}S_9$. Presence of eutectic (SnS–Cu_2S), SnS and Cu_2ZnSnS_4 and Cu_2SnS_3. See Fig. 2b.
31	$Cu_2Zn_6SnS_9$	1010–960 °C and quenching	$Cu_{2-2x}Zn_{6+3x}Sn_{1-x}S_9$	5.0	43.6	2.3	49.1	More than 95% $Cu_{2-2x}Zn_{6+3x}Sn_{1-x}S_9$. Presence of eutectic (SnS–Cu_2S), SnS and Cu_2ZnSnS_4.
32	$Cu_2Zn_6SnS_9$	1010–960 °C and quenching	$Cu_{2-2x}Zn_{6+3x}Sn_{1-x}S_9$	8.5	38.3	4.0	49.2	Around 90% $Cu_{2-2x}Zn_{6+3x}Sn_{1-x}S_9$. Presence of eutectic (SnS–Cu_2S), SnS and Cu_2ZnSnS_4 and Cu_2SnS_3.

Table 1 (*continued*)

33	$Cu_2Zn_6SnS_9$	20–1100 °C (5°/min) and slow cooling	$Cu_{2-2x}Zn_{6+3x}Sn_{1-x}S_9$. Cu_2ZnSnS_4	u.d 23.8	u.d 16.2	u.d 11.8	u.d 48.2	Around 40% Cu_2ZnSnS_4. The $Cu_{2-2x}Zn_{6+3x}Sn_{1-x}S_9$ is under decomposition (see text); ZnS and SnS are also present.
34	$Cu_2Zn_6SnS_9$	DTA analysis: 20–1100 °C (5°/min) and 1100–20 °C (5°/min)	$Cu_{2-2x}Zn_{6+3x}Sn_{1-x}S_9$. Cu_2ZnSnS_4	u.d 22.9	u.d 16.9	u.d 11.4	u.d 48.8	Around 50% Cu_2ZnSnS_4. The $Cu_{2-2x}Zn_{6+3x}Sn_{1-x}S_9$ is under decomposition (see text); ZnS, SnS and eutectic (SnS–Cu_2S) are present.
35	$Cu_2Zn_6SnS_9$	DTA analysis: 20–1100 °C (5°/min) and 1100–20 °C (5°/min)	$Cu_{2-2x}Zn_{6+3x}Sn_{1-x}S_9$ Cu_2ZnSnS_4	u.d 23.7	u.d 15.6	u.d 12.1	u.d 48.6	Around 50% Cu_2ZnSnS_4. The $Cu_{2-2x}Zn_{6+3x}Sn_{1-x}S_9$ is under decomposition (see text); ZnS, SnS and eutectic (SnS–Cu_2S) are present. See Fig. 4.
36	$Cu_{18}Zn_{82}Sn_9S_{109}$	1010–960 °C and quenching	$Cu_{2-2x}Zn_{6+3x}Sn_{1-x}S_9$ Cu_2ZnSnS_4	5.8 24.9	42.1 13.8	2.8 12.2	49.3 49.1	85% $Cu_{2-2x}Zn_{6+3x}Sn_{1-x}S_9$. Presence of eutectic (SnS–Cu_2S), SnS, Cu_2ZnSnS_4 and Cu_2SnS_3.
37	$Cu_{18}Zn_{82}Sn_9S_{109}$	1010–960 °C and quenching	$Cu_{2-2x}Zn_{6+3x}Sn_{1-x}S_9$ Cu_2ZnSnS_4	7.7 25.2	39.8 13.9	3.7 12.4	48.8 48.5	90% $Cu_{2-2x}Zn_{6+3x}Sn_{1-x}S_9$. Presence of eutectic (SnS–Cu_2S), SnS and Cu_2ZnSnS_4.
38	$Cu_2Zn_{18}SnS_2$	1010–960 °C and slow cooling	$Cu_{2-2x}Zn_{6+3x}Sn_{1-x}S_9$ Cu_2ZnSnS_4	3.8 24.1	45.0 14.6	1.8 12.3	49.4 49.0	90% $Cu_{2-2x}Zn_{6+3x}Sn_{1-x}S_9$. Presence of eutectic (SnS–Cu_2S) and Cu_2ZnSnS_4.

u.d = under decomposition.

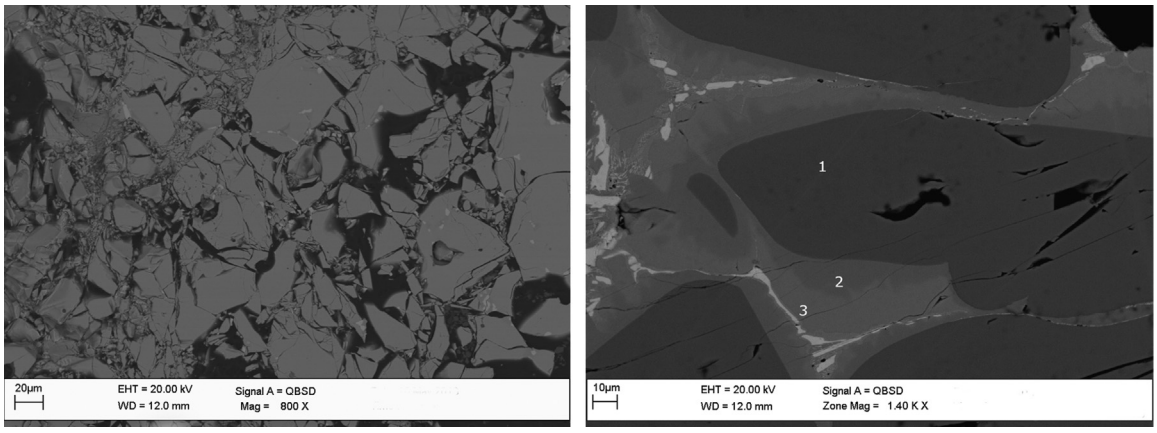

Fig. 1. SEM image (BSE mode) of samples # 5 and # 8 (see Table 1): (a, # 8) almost one-phase Cu_2ZnSnS_4 sample obtained by solid state reaction; (b, # 5) a multi-phase sample obtained through the liquid phase: big crystals of $Cu_{2-2x}Zn_{6+3x}Sn_{1-x}S_9$ (dark grey – 1), surrounded by Cu_2ZnSnS_4 (grey – 2) and Cu_2SnS_3 (light grey – 3) together with Cu_2S–SnS eutectic mixture.

analyses were performed for each phase in various portions of the sample both on area and spots and the final composition was averaged from the quantitative results. Generally for each element an error within ±0.5 at% was ascribed. Differential thermal analyses have been performed on selected samples using a SETARAM instrumentation TG-DTA/DSC.

3. Results and discussion

The list of the prepared samples together with the synthesis conditions and the SEM/EDS analysis on the detected phases is shown in Table 1. The wide variety of employed thermal treatments can be noticed.

Almost one-phase Cu_2ZnSnS_4 (CZTS) samples were obtained using the solid state synthesis based on the heat treatments performed by Choubrac et al. [8] (samples # 7–10). The typical microstructure of the SEM image (BSE mode) of a Cu_2ZnSnS_4 one-phase sample in Fig. 1a (sample # 8) is displayed: the grey quaternary phase is surrounded by black cracks and holes which are due to his high brittleness. In samples having the same starting composition (Cu_2ZnSnS_4: 25 at% Cu, 12.5 at% Zn, 12.5 at% Sn and 50 at% S) but undergoing high temperature treatments through the liquid phase (samples # 1, 3–6, 11–13) several phases have been detected. As an example, Fig. 1b (sample # 5) shows the microstructure of a multi-phase sample: big crystals of $Cu_{2-2x}Zn_{6+3x}Sn_{1-x}S_9$ (dark grey – 1), surrounded by Cu_2ZnSnS_4 (grey – 2) and Cu_2SnS_3 (light grey – 3) together with Cu_2S–SnS eutectic mixture. Presence of the "$Cu_{2-2x}Zn_{6+3x}Sn_{1-x}S_9$" quaternary phase was observed in samples # 1, 3–6, 11–38. The SEM/EDS analyses were performed for the $Cu_{2-2x}Zn_{6+3x}Sn_{1-x}S_9$ phase in more than 40 points in each sample and the concentration values comes from their average. This phase was not reported up to now in the literature; the different compositions of this new quaternary phase detected in our samples by SEM/EDS analysis suggest for the $Cu_{2-2x}Zn_{6+3x}Sn_{1-x}S_9$ a homogeneity range corresponding to $0 < x < 0.74$ (see Table 1). Almost one-phase samples of the new quaternary phase were prepared both by solid state reaction (samples # 24 and 25) and through the liquid phase (samples # 30–32) starting from samples having the $Cu_2Zn_6SnS_9$ nominal composition (11.1 at% Cu, 33.3 at% Zn, 5.6 at% Sn and 50.0 at% S). Fig. 2a (sample # 24) shows the SEM (BSE mode) image of a one-phase $Cu_{2-2x}Zn_{6+3x}Sn_{1-x}S_9$ sample obtained by solid state synthesis: the quaternary phase (grey phase) is more than 95%, nevertheless a small amount of secondary white phase is detectable. The microstructure of a sample obtained with the high temperature treatment is displayed in Fig. 2b (sample # 30) and, also in this case, an almost one-phase sample of the new quaternary one $Cu_{2-2x}Zn_{6+3x}Sn_{1-x}S_9$ was obtained (grey phase). The bright secondary phase is less than 5% and the brittleness is evidenced by the black cracks and holes.

A preliminary analysis on the SEM/EDS experimental data obtained on samples having the Cu_2ZnSnS_4 starting composition but subjected to different thermal treatments (samples # 1–13), suggested that the formation of the new quaternary phase $Cu_{2-2x}Zn_{6+3x}Sn_{1-x}S_9$ could occur between 1050 °C and 800 °C.

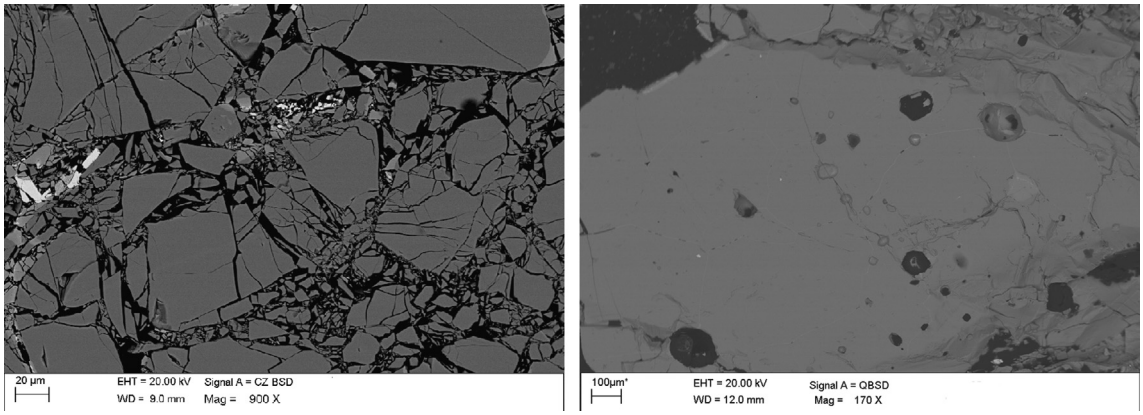

Fig. 2. SEM image (BSE mode) of one-phase $Cu_{2-2x}Zn_{6+3x}Sn_{1-x}S_9$ samples (# 24 and # 30 in Table 1) obtained (a) by solid state reaction and (b) through the liquid phase. Large grains (400–600 µm) of $Cu_{2-2x}Zn_{6+3x}Sn_{1-x}S_9$ phase together with a very small amount (less than 5%) of secondary phases.

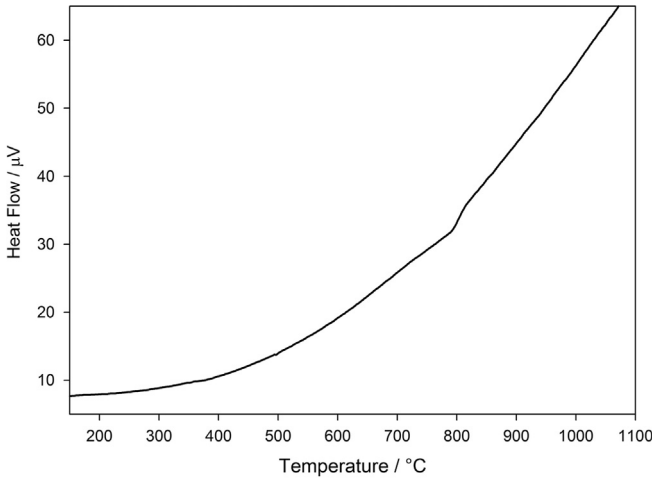

Fig. 3. Differential Thermal Analysis (DTA) curve obtained for sample # 35 (Table 1) on heating from 20 °C to 1100 °C (heating rate 5°/min).

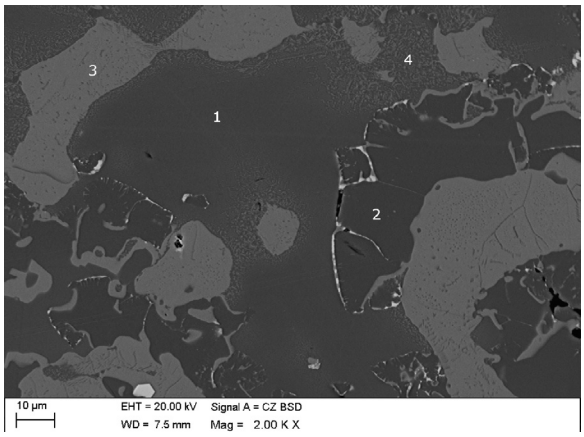

Fig. 4. SEM image (BSE mode) of the sample # 35. The under way decomposition of the $Cu_{2-2x}Zn_{6+3x}Sn_{1-x}S_9$ phase can be observed into the region labelled with 4. The $Cu_{2-2x}Zn_{6+3x}Sn_{1-x}S_9$ phase (grey – 1) decomposes into ZnS (dark grey – 2) and Cu_2ZnSnS_4 (light grey – 3), see text. A few black holes are clearly visible in the image.

Indeed, this phase was not detected in samples treated ad lower temperatures (up to 800 °C; samples # 2, 7–10) but appears when the heat treatments reach higher temperatures (samples # 3–6, 11–13).

Furthermore, the analysis of SEM/EDS results obtained on a one-phase $Cu_{2-2x}Zn_{6+3x}Sn_{1-x}S_9$ (sample # 25) sample subjected after the synthesis to cyclic thermal treatment from 20 °C to 1100 °C at 5 °C/min heating rate, suggested the existence of a possible eutectoidal reaction (see comments on sample # 33).

In order to define the stability temperature range of the new quaternary phase, one-phase $Cu_{2-2x}Zn_{6+3x}Sn_{1-x}S_9$ samples (~20 mg) were sealed in a small quartz tube and subjected to a DTA analyses with a thermal cycle from 20 °C to 1100 °C at 5 °C/min heating rate (samples # 34 and # 35). A small effect (due to the small amount of sample employed) at around 790 °C was observed, as shown in Fig. 3. We should underline that before the DTA analysis the microstructure of samples # 34 and # 35 was similar to that reported in Fig. 2a, showing very large crystals of $Cu_{2-2x}Zn_{6+3x}Sn_{1-x}S_9$ phase.

The SEM/EDS analyses performed on these samples after DTA confirmed the decomposition of the new phase into ZnS and Cu_2ZnSnS_4, as shown in the BSE image reported in Fig. 4 (sample # 35). The big $Cu_{2-2x}Zn_{6+3x}Sn_{1-x}S_9$ crystals have been replaced by ZnS (dark grey – 2) and Cu_2ZnSnS_4 (light grey – 3); nevertheless under the heating and cooling rate employed the decomposition of the new phase was not complete. Indeed, the region labelled with 1, shows the undecomposed $Cu_{2-2x}Zn_{6+3x}Sn_{1-x}S_9$ phase (grey phase) and in the region labelled with 4 the underway decomposition is evident. These experimental results confirm the existence of $Cu_{2-2x}Zn_{6+3x}Sn_{1-x}S_9$ as a new phase, and rule out the hypothesis that the $Cu_{2-2x}Zn_{6+3x}Sn_{1-x}S_9$ composition corresponds to an extension of the ZnS phase into the quaternary system.

4. Conclusions

More than 35 samples were prepared at different compositions that lie along the ZnS–Cu_2SnS_3 section by using peculiar heat treatments to study the bulk properties of the Cu–Zn–Sn–S photovoltaic material. The existence of a new phase having the $Cu_{2-2x}Zn_{6+3x}Sn_{1-x}S_9$ ($0 < x < 0.74$) composition was determined. The peculiarities of the microstructure and the DTA analysis show that the $Cu_{2-2x}Zn_{6+3x}Sn_{1-x}S_9$ phase decomposes at around 790 °C by eutectoidal decomposition into ZnS and Cu_2ZnSnS_4. Considering the sluggishness of the solid state reactions, we can observe that it is still ongoing; probably a longer annealing will allow achieving the complete decomposition. The presence of this phase suggests a modification of the ZnS–Cu_2SnS_3 section proposed by Olekseyuk et al. [7].

Acknowledgements

Diego Colombara acknowledges funding from the EPSRC (Engineering and Physical Sciences Research Council) (Supergen: Photovoltaic Materials for the 21st Century EP/F029624/1).

References

[1] Green MA, Emery K, Hishikawa Y, Warta W, Dunlop ED. Solar cell efficiency tables (version 43). Prog Photovolt Res Appl 2014;22:1–9.
[2] Peter LM. Towards sustainable photovoltaics: the search for new materials. Philos Trans R Soc A 2011;369:1840–56.
[3] Colombara D, Dale P, Peter L, Scragg J, Siebentritt S. Thin-film photovoltaics based on earth-abundant materials. In: Nozik AJ, Conibeer G, Beard MC, editors. Advanced concepts in photovoltaics, Chapter 5. Cambridge: Royal Society of Chemistry; 2014. p. 118–85.
[4] Suryawanshi MP, Agawane GL, Bhosale SM, Shin SW, Patil PS, Kim JH, et al. Mater Technol: Adv Perform Mater 2013;28:98–109.
[5] Delbos S. Këesterite thin films for photovoltaics: a review. EPJ Photovolt 2012;3:35004.
[6] Polizzotti A, Repins IL, Noufi R, Wei SH, Mitzi DB. The state and future prospects of kesterite photovoltaics. Energy Environ Sci 2013;6:3171–82.
[7] Olekseyuk ID, Dudchak IV, Piskach LV. Phase equilibria in the Cu_2S–ZnS–SnS_2 system. J Alloy Compd 2004;368:135–43.
[8] Choubrac L, Lafond A, Guillot-Deudon C, Moëlo Y, Jobic S. Structure flexibility of the Cu_2ZnSnS_4 absorber in low-cost photovoltaic cells: from the stoichiometric to the copper-poor compounds. Inorg Chem 2012;51:3346.